Structural dynamics in the C terminal domain homolog of orange carotenoid protein reveals residues critical for carotenoid uptake

Dvir Harris, Fernando Muzzopappa, Fabian Glaser, Adjele Wilson, Diana Kirilovsky, Noam Adir

Journal Pre-proof

Structural dynamics in the C terminal domain homolog of orange carotenoid protein reveals residues critical for carotenoid uptake

Dvir Harris, Fernando Muzzopappa, Fabian Glaser, Adjélé Wilson, Diana Kirilovsky, Noam Adir

PII: S0005-2728(20)30064-5

DOI: https://doi.org/10.1016/j.bbabio.2020.148214

Reference: BBABIO 148214

To appear in: *BBA - Bioenergetics*

Received date: 2 October 2019

Revised date: 19 March 2020

Accepted date: 27 April 2020

Please cite this article as: D. Harris, F. Muzzopappa, F. Glaser, et al., Structural dynamics in the C terminal domain homolog of orange carotenoid protein reveals residues critical for carotenoid uptake, *BBA - Bioenergetics* (2020), https://doi.org/10.1016/j.bbabio.2020.148214

Structural dynamics in the C terminal domain homolog of Orange Carotenoid protein reveals residues critical for carotenoid uptake

Dvir Harris[1,2], Fernando Muzzopappa[3], Fabian Glaser[4], Adjélé Wilson[3], Diana Kirilovsky[3,*] and Noam Adir[1,2,*]

[1] *Schulich Faculty of Chemistry, Technion, Haifa 3200003, Israel.*

[2] *Grand Technion Energy Program (GTEP), Technion, Haifa 3200003, Israel.*

[3] *Université Paris-Saclay, CNRS, CEA, Institute for Integrative Biology of the Cell (I2BC), 91198 Gif sur Yvette, France*

[4] *Lorry I. Lokey Interdisciplinary Center for Life Sciences and Engineering, Technion-Israel Institute of Technology, Haifa, Israel.*

* Corresponding authors.

Prof. Noam Adir, Schulich Faculty of Chemistry, Technion, Technion City Haifa 32000 Israel. Email: noam@ch.technion.ac.il. ORCID ID 0000-0003-2766-8409

Dr. Diana Kirilovsky, *Université Paris-Saclay, CNRS, CEA, Institute for Integrative Biology of the Cell (I2BC), , 91198 Gif sur Yvette, France* Diana.KIRILOVSKY@cea.fr. ORCID ID 0000-0003-2146-3103

Keywords: X-ray crystallography, cyanobacteria, ligand transfer, photoprotection, molecular dynamics, mutagenesis.

Abstract

The structural features enabling carotenoid translocation between molecular entities in nature is poorly understood. Here, we present the three-dimensional X-ray structure of an expanded oligomeric state of the C-terminal domain homolog (CTDH) of the orange carotenoid protein, a key water-soluble protein in cyanobacterial photosynthetic photo-protection, at 2.9 Å resolution. This protein binds a canthaxanthin carotenoid ligand and undergoes structural reorganization at the dimeric level, which facilitates cargo uptake and delivery. The structure displays heterogeneity revealing the dynamic nature of its C-terminal tail (CTT). Molecular dynamics (MD) simulations based on the CTDH structures identified specific residues that govern the dimeric transition mechanism. Mutagenesis based on the crystal structure and these MD simulations then confirmed that these specific residues within the CTT are critical for carotenoid uptake, encapsulation and delivery processes. We present a mechanism that can be applied to other systems that require cargo uptake.

Keywords: X-ray crystallography, cyanobacteria, ligand transfer, photoprotection,

molecular dynamics, mutagenesis

1. Introduction

Photosynthetic organisms utilize carotenoid molecules to carry out photosynthesis in a highly coordinated manner, as carotenoids have critical roles in both excitation energy transfer and excitation energy quenching, facilitating the fine-tuning of the intricate photosynthetic process [1,2]. Carotenoids are often found as bound-ligands of hydrophobic, membrane-integrated complexes such as photosynthetic light harvesting antenna and reaction centres (RC)[1] [3–5]. Cyanobacteria, which are the most ancient oxygenic photosynthetic organisms [6,7], utilize carotenoids in additional functionalities. Cyanobacteria express several water-soluble, carotenoid-binding proteins, which play major roles in maintaining photosynthesis [8,9]. One of the most prominent water-soluble carotenoid binding proteins is the orange carotenoid protein (OCP). When OCP is activated, it is the main participant in a non-photochemical protection mechanism against high light irradiation [10,11]. Cyanobacteria may become exposed to an elevated photon flux arriving at the RC of photosystem II, leading to over-reduction of the down-stream intermediates in the electron transfer chain. The resulting bottleneck of electrons can lead to the formation of deleterious reactive oxygen species (ROS). Under high light irradiation, cyanobacteria utilize the OCP to diminish reaction centre excitation, thus avoiding the formation of ROS [12,13]. The OCP is a 35kDa, photo-activated protein. Under normal light conditions, the OCP is inactive (OCP^O state, orange). In this state, the two main domains of OCP – the N-terminal domain (NTD) and the C-terminal domain (CTD), encapsulate a keto-carotenoid in a non-covalent fashion [14,15]. An N-terminal extension (NTE) flanks the CTD, stabilizing OCP^O. The C-terminal tail (CTT) is bound to the main body of the CTD through interactions with its β-sheet domain [16,17].

[1]Abbreviations: AU, asymmetric unit; CAN, canthaxanthin; CTD, C-terminal domain; CTDH. C-terminal domain homologue of the OCP; CTT, C-terminal tail; EET, excitation energy transfer; HCP, helical carotenoid protein; LHC, light harvesting complex; MD, molecular dynamics; MR, molecular replacement; NPQ, non-photochemical quenching; NTD, N-terminal domain, NTE, N-terminal extension; NTF2, nuclear transport factor 2; OCP, orange carotenoid protein; PBS, phycobilisome; RC, reaction center; ROS, reactive oxygen species; RPE65, retinal pigment epithelium 65 enzyme

Upon exposure of the OCP to high light, the active OCP state (OCP^R, red) is generated. Photon absorption by the carotenoid induces a conformational change that destabilizes the CTD-carotenoid hydrogen bonding, resulting in a 12Å translocation of the carotenoid into a designated tunnel in the NTD [18–20]. Consequently, the NTE-CTD interaction is disrupted, leading to a complete separation of the carotenoid-binding NTD (holoNTD) and carotenoid-free CTD (apoCTD), leaving them connected by a flexible loop [14,15,21,22]. It is only then the OCP^R can interact with the Phycobilisome (PBS) light harvesting antenna, via holo-NTD. This interaction induces structural alterations to the PBS complex, hampering its highly efficient excitation energy transfer (EET) towards the RC [16,23–26]. The structure of the OCP^O and the structure of holoNTD (in some instances referred to as the red carotenoid protein; RCP), have been determined by X-ray crystallography [18,27]. Recently, genes encoding for proteins that are homologous to the individual domains of the OCP were identified [17,28–30]. These homologs are divided into either N-terminal domain homologs (termed helical carotenoid protein, HCP, for their all α-helical structure) or C-terminal domain homologs (CTDH). Interestingly, while nine clades of HCPs were found in all known cyanobacterial genomes, (HCP1-9), only two clades of CTDH (CTDH1-2) were identified [30]. In *Anabaena* PCC7120 , which serves as a canonical organism for the study of the functions of OCP domain homologs, only the genes encoding for HCP1-4 and CTDH2 exist. In addition to EET quenching, the NTD of OCP has also been shown to have the potential to directly quench singlet oxygen (one of the most potent ROS species). HCPs were also demonstrated to possess this duel-quenching function [28,31,32]. CTDHs were shown to function as a carotenoid relay (as well as ROS quencher), acquiring this hydrophobic molecule either from membranes or from HCP1 (the only NTD homolog incapable of inducing any type

of quenching, of EET or of ROS) or from the activated OCP^R state, and deliver it to either HCP2-4 or OCP. Moreover, it was shown that while *Anabaena* CTDH (AnaCTDH) or the CTD of OCP (obtained by heterologous expression and called COCP) can act as a dimer encapsulating carotenoids. *Thermosynechococcus elongatus* CTDH (TeCTDH) can function as a monomer which binds a carotenoid without encapsulation with a second monomer [33–37]. We have recently unraveled some of the details of the carotenoid uptake and delivery cycle by AnaCTDH. This was achieved by solving the structure of apoCTDH in the presence of 2M urea and complementing this data with SAXS analysis and uptake experiments with site-specific mutants[33]. Structural homology comparison revealed that the CTD of OCP, and the CTDH belong to the nuclear transport factor 2 (NTF2) superfamily fold (Pfam02136)[15]. We have also previously demonstrated that the CTT of the CTDH facilitates both carotenoid uptake and delivery, and suggested that the CTDH undergoes a dimeric reorganization from a back-to-back apoCTDH mode (which uptakes a carotenoid molecule) to a head-to-head holoCTDH form (which encapsulates the now-bound carotenoid until delivered to HCP2-4/OCP)[33]. However, two major questions remained unsolved - ***i***. How does the CTT facilitate carotenoid uptake and delivery, and are both processes performed by a similar mechanisms? ***ii***. What is the mechanism by which the dimers reorganize? We now provide new structural, computational and biochemical data that give new insight into these two questions. The overall mechanism described here may have far-reaching consequences, beyond the OCP in cyanobacteria system, as will be discussed later in this paper.

2. Materials and Methods

2.1 Apo- and holo-CTDH and HCP production, isolation, and purification

Construction of the plasmid pCDF-CTDHana with His-tag in the C-terminus, carrying the CTDH from *Anabaena* PCC7120 (gene *all4940*) used to overexpress the Apo-CTDH for crystallization was previously reported[36]. The constructs for the overexpression of *Anabaena* PCC7120 HCP1 (pCDF-HCP1), HCP4 (pCDF-HCP4)[28], CTDH-C103F and CTDH-C103FΔCTT (both with N-terminus His-tag)[33] have been previously described. The point mutations L128D and L137D were introduced by directed mutagenesis, using the pCDF-CTDHanaC103F plasmid as template and the following mismatching primers: L128D_fw: CCCAAATTAAACTCGACGCTTCTCCCCAAGAGTTACTGGC (for L128D), L128D_rv: GCCAGTAACTCTTGGGGAGAAGCGTCGAGTTTAATTTGGG (for L128D), L137D_fw: CCCCAAGAGTTACTGGCTGACCGTCGTGAACAG (for L137D), L137D_rv: CTGTTCACGACGGTCAGCCAGTAACTCTTGGGG (for L137D). The production and isolation of apo and holo-AnaCTDHs (WT and mutants) was performed as previously described [36].

2.2 Size Exclusion Chromatography (SEC)

Purified proteins (10 mM) were injected into a Superdex Increase 75 10/300 column (GE Healthcare) equilibrated with 40mM Tris-HCl pH 8, 150mM NaCl. The Akta FLPC system was equipped with a UV detector at 280 nm and 560 nm and was set at a flow rate of 0.8 mL/min. The Gel Filtration Calibration Kit LMW (GE Healthcare) was used to calibrate the column.

2.3 Crystallization and data collection

Crystals of the expanded oligomeric state of apoCTDH were obtained according to Harris et al. [33]; briefly, crystals were obtained at 20°C by hanging drop diffusion method when grown in 1.26M NaH_2PO_4*H_2O, 0.14M K_2HPO_4, pH=5 (optimized following use of an INDEX HT screen, Hampton Research). A full description of crystal morphology and data processing pipeline can be found in Harris et. al [33]. Molecular replacement was carried out using Phaser [46], using the structure of one apoCTDH monomer obtained in the presence of 2M urea

(PDB code 6FEJ), with truncated CTT. Reciprocal space structural refinement was performed using Phenix [47] and manual modifications were made using Coot[48]. PDBREDO server[49] was utilized to minimize errors prior to deposition to the PDB. The structure was then carefully examined and compared to other structures using PyMoL [50]. The final structure was deposited in the PDB under the accession code 6S5L.

2.4 Molecular Docking

The SDF format of the ligand was downloaded, charged and minimized for docking by *Maestro Schrodinger*[51] *V11.9* software, using OPLS2005 force field. Protein target processed by *AutoDockTools (ADT)* and gasteiger charges were assigned to the target [52]. Docking was then performed between the carotenoid ligand from 4XB4 and the target CTDH structure (6FEJ) – by the *AutoDock* docking software, using the Lamarckian genetic algorithm. We ran 200 docking simulations with 25,000,000 energy evaluations per run and a grid spacing of 0.375 Å. The lowest energy pose was then chosen for starting molecular dynamics simulation.

2.5 Molecular dynamics setup

The lowest energy docking pose carotenoid conformation was then pre-processed with Antechamber [53] to calculate charges and atom types with GAFF forcefield [54]. All atom types were recognized by the forcefield. Then, *Tleap* program (version 18 Amber16 suite), processed the protein and ligand, with the FF14SB force field for the protein, GAFF for the ligand and TIP3P for water and added the complex into a truncated solvated octahedron box with a 10 Å nonbonded cutoff, generating coordinates and parameter input files for MD simulation [55]. This process was applied for several different starting conformations and configurations (i.e. holo and apo CTDH) (see below) to obtain all MD data.

2.6 Molecular Dynamics protocol

The equilibration protocol consisted of an initial minimization and several steps of heating, and a gradual reduction of initial positional restraints[56]. Equilibration of box volume was carried on at constant pressure while production is run at constant volume. Equilibration consisted of a total of 8 ns of MD with a time step of 1fs (stages 1-8) and 2 fs (stage9). First a minimization of water and added H atoms (stage 1); 1 ns of MD heating, using restraints on every atom at constant volume (NVT ensemble) (stage2); Then 1 ns of MD at constant pressure (NPT ensemble) and constant temperature to adjust the density of water with full restraint on protein (stage 3); Then 1 ns of MD with lower restraints at NPT (stage 4); Then a second minimization of the side chains (stage 5); Then three stages of 1ns MD at constant pressure with decreasing restraints on backbone (stages 6-8); And finally a 2 ns unrestrained run at NTP (stage 9).

The production MD was then performed at NVT for 2000 ns, which was found to be sufficient for reaching convergent results (based on rmsd). Hydrogen-mass repartitioning was used to increased time step to 4 fs (dt=0.004). Periodic boundary conditions and Ewald sums (grid spacing of 1 Å) were used to treat long range electrostatic interactions. During production runs, netCDF (Network Common Data Form) trajectory files for each ns of MD were created (writing frequency of 500 and 500,000 steps in total) were performed.

All analyses were performed using CPPTRAJ module [57], while structural snapshots were extracted from each simulation using the Visual Molecular Dynamics software [58].

2.7 MM-GBSA and MM-PBSA

Molecular docking results from AutoDock could be used to compute binding free energy. However, the lack of sampling results in an inaccurately binding free energy estimate. It is therefore common to evaluate the binding free energy with more accurate method including the MM/PBSA method [59]. Thus we used MM-

GBSA and MM-PBSA free energy calculations to compute the ΔG for the CTDH monomer-monomer interface using Amber built in MMPBSA.py script [40]. This script computes the end-state free energy of the monomer-monomer binding from an ensemble of representative structures obtained from MD by taking into account the solvation energies of the interacting molecules in addition to molecular mechanics (MM) energies. The contribution of polar solvation energy is calculated with the implicit solvent model (GB or PB) whereas the nonpolar part of the solvation energy is computed from the solvent accessible surface area (SASA). The free energies of binding (ΔG binding) can be estimated from the free energies of the reactants. Here, we used 500 snapshots collected from the last 10 ns (spaced by 20 ps) of the production MD simulation to compute MM-PB(GB)SA and free energy decomposition energies.

2.8 MD analysis tools

We used *CPPTRAJ* [57] to analyze the trajectory data and calculation of root mean squared fluctuation (RMSF) of specified atoms/residues and root mean square deviation (RMSD), and monitoring key distances, hydrogen bonds etc. during the simulation. Hydrogen bond criteria applied a donor–acceptor distance cutoff of 3.5 Å and a 120° cutoff for the donor-hydrogen-acceptor angle.

For trajectory visualization we used tools in *Visual Molecular Dynamics (VMD)* software[58] for structures that were extracted every 10 ps for each 1000 ns trajectory. Figures from dynamics simulation were created by ChimeraX[60] (Molecular graphics and analyses performed with UCSF ChimeraX, developed by the Resource for Biocomputing, Visualization, and Informatics at the University of California, San Francisco, with support from NIH R01-GM129325 and P41-GM103311)

2.9 Absorbance measurements and experiments of carotenoid transfer

Absorbance spectra and kinetics of carotenoid transfer were measured in a Specord S600 spectrophotometer (Analytic Jena). To study the kinetics of carotenoid transfer holo-CTDH and apo-HCP4 were incubated in a ratio = 1 holo-CTDH dimer to 2.5 apo-HCP4, and holo-HCP1 and apo-CTDH were incubated in a ratio = 1 HCP1 to 1 monomeric apo-CTDH. The spectral changes were followed during 1 hour in darkness at 23 °C. The kinetics were obtained from the changes in absorbance at 600 nm. Spectral deconvolution was performed to determine the percentage of carotenoid transfer, using Excel to fit the data to the sum of reference spectra (Holo-CTDH and Holo-HCP) as it was previously described [36]. The holoprotein reconstitution upon carotenoid uptake from membranes was study by incubating 12 µM Apo-CTDH-dimers with canthaxanthin-containing membranes (48 µM CAN (measured by acetone extraction, ε_{466nm} = 124080 $M^{-1}cm^{-1}$)) for 1 hour at 33°C in darkness. The percentage of holo-protein formed was determined by comparing the spectra of 100% holo-proteins (at 12 µM) to those of the supernatant.

3. Results

3.1 The ApoCTDH structure in absence of urea. Initial attempts to solve the three-dimensional structure of the ApoCTDH in crystals containing an expanded oligomeric state of apoCTDH were unsuccessful [33]. This was most likely due to the large number of monomers in the AU and a significant deviation in structure with potential CTD models (3MG1 or 5UI2). Disassembly of the expanded oligomer by treatment with 2M urea released dimeric CTDH (see Methods section for details), which resulted in the apoCTDH structure (6FEJ), that demonstrated a dramatic change in the position of the CTT as compared to its position in the

OCP [33]. We then were able to utilize this structure as the MR search model for the expanded oligomeric state of apoCTDH. The results of structure determination (PDB code 6S5L) is shown in figure 1 and the crystallographic data collection and refinement parameters are given in table S1.

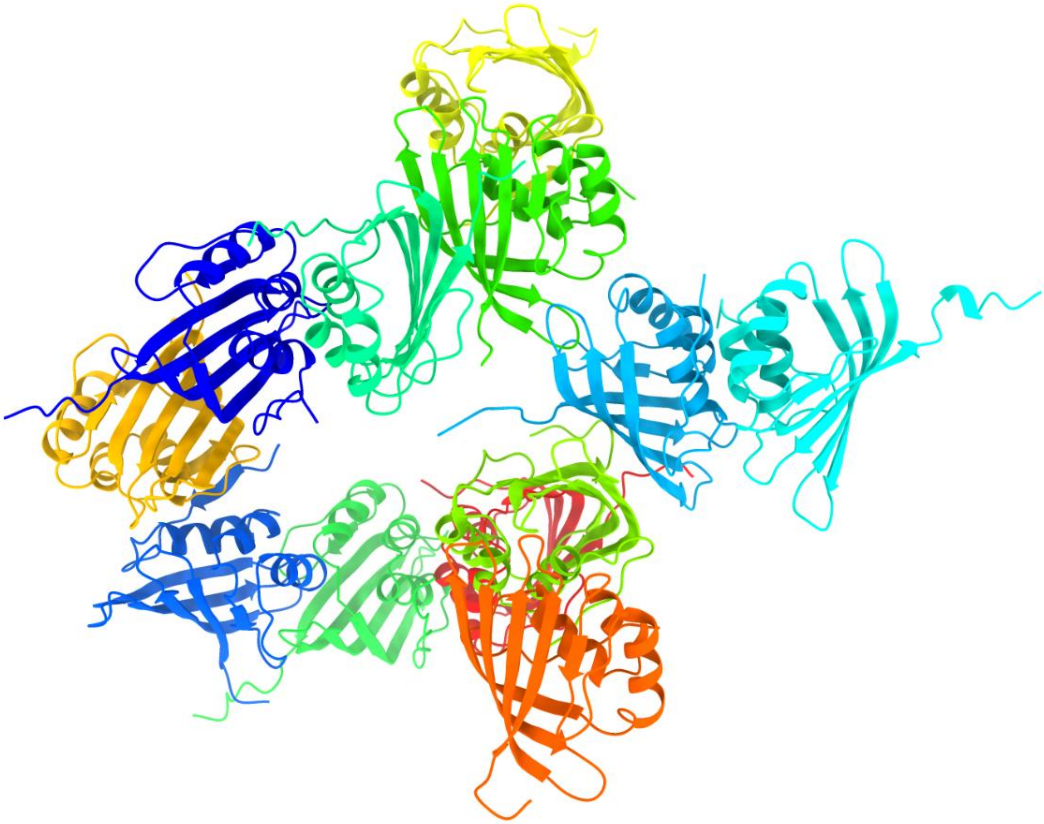

Figure 1. Expanded oligomeric apoCTDH crystal structure. Twelve apoCTDH monomers were identified in the asymmetric unit. All monomers form interfaces with other monomers leading to both face-to-face and back-to-back type dimers, as seen in the 6FEJ structure. The critical CTT is found in different orientations. All molecular graphics were created using ChimeraX[60].

The 6S5L crystal structure shows the presence of a dodecamer in the asymmetric unit. As this expanded oligomeric state adopts a quaternary structure without clear non-crystallographic symmetry, we chose to further investigate whether structural differences between apoCTDH monomers emerged as a result of the presence or absence of 2M urea or different buffers. To clearly identify the different conformations of the CTDH, a superposition of the 12 individual apo-protomers, a 6FEJ apo-monomer (in 2M urea) and the 5UI2 holo-monomer (holoCTD of OCP^{O}), was performed, as displayed in Figure 2.

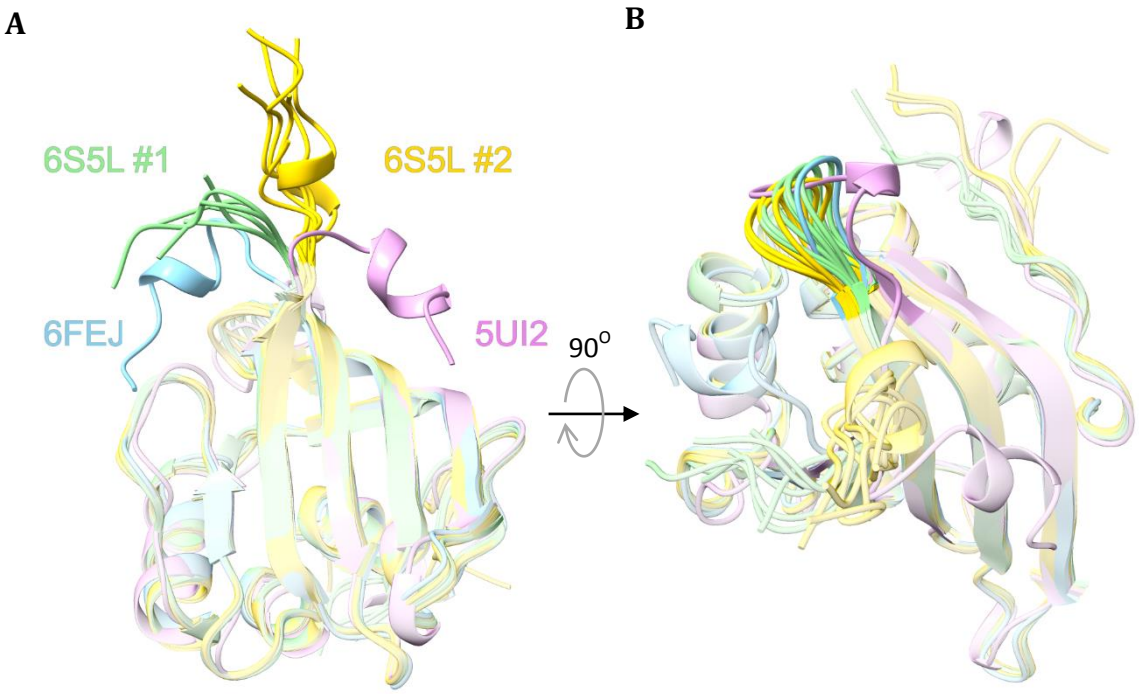

Figure 2. Superposition of all CTD(H) structures. (A) Superposition of HoloCTD of OCP^{O} (violet, PDB code 5UI2, carotenoid is omitted for clarity), 2M urea apoCTDH structure (cyan, PDB code 6FEJ) and the 12 apo-protomers of the 6S5L CTDH structure described here in the absence of urea (green and yellow) demonstrates the different positions CTT adopts. (B) Same as A, but in an orientation (90^{o} rotation as indicated) that shows the variability in the β5/β6

The expanded oligomeric state 6S5L structure reveals that the 12 monomers present in the asymmetric unit can be divided into two populations (comprising 6 monomers each, colored in green and yellow in Fig. 2), according to their relative CTT position. Previously, we suggested that the incorporation of a carotenoid into its designated cavity in the CTDH protein releases the CTT from its internal position (Fig. 2, cyan) to adopt its open position (Fig. 2, violet) [33]. However, as revealed in the 6S5L structure, the CTT can assume two additional positions (Fig. 2, green and yellow), being intermediate CTT conformations, with respect to the two positions already identified. In addition, the β5/β6 loop also displays more subtle dynamics, when compared to the CTT (Fig. 2B), adopting more internal positions (relative to the protein cavity) as compared to these loops in the 6FEJ/5UI2/3MG1 structures. Interestingly, in the presence of 2M urea, the two monomers in the AU are almost identical (RMSD of 0.235Å). The two CTTs are also in very similar positions, folded back towards the carotenoid-binding cavity.

In the absence of urea, one CTT orientation (fig. 2A, yellow) is found mid-way between the open and closed conformations, parallel to the carotenoid-binding cavity, while the other one (fig. 2A, green) is found between the closed and the parallel orientation, closer to the closed conformation.. The crystal packing interactions vary between the 12 monomers, however CTTs in both orientations are found in these positions without stabilization by nearby monomers. We thus conclude that all three positions of apoCTDH seen in Fig. 2 are independently stable. The only difference between the 6S5L and the 6FEJ structures are the absence or presence of 2M urea and small changes in the crystallization liquor. Considering this, and that the crystal lattice contacts do not consistently stabilize the same surface areas of the protein monomers, we deduce that these domains have significant dynamics, between the three stable apo-intermediates.

Based on the 6FEJ structure, we previously proposed that the back-to-back apo-dimer could flip into a head-to-head conformation, upon carotenoid binding [33]. We therefore aimed to further investigate and corroborate this process from an atomistic-mechanistic point of view. When we superimpose (Fig. 2) all known monomeric configurations of CTD(H), we see a dynamic motion indicating CTT flexibility, stabilized at specific terminal and intermediate states. We thus decided to utilize molecular dynamics (MD), to shed new light upon this process of CTT translocation and its implications.

3.2 Predicting apo- and holo- CTDH conformational changes using molecular dynamics

To simulate the effect of carotenoid binding on the dynamicity of the CTT, the canthaxanthin (CAN) ligand (carved from the RCP structure, 4XB4) was docked into the 6FEJ structure by Autodock [38]. Interestingly, although partially blocked by the CTT, during the docking procedure the CAN molecule penetrated into

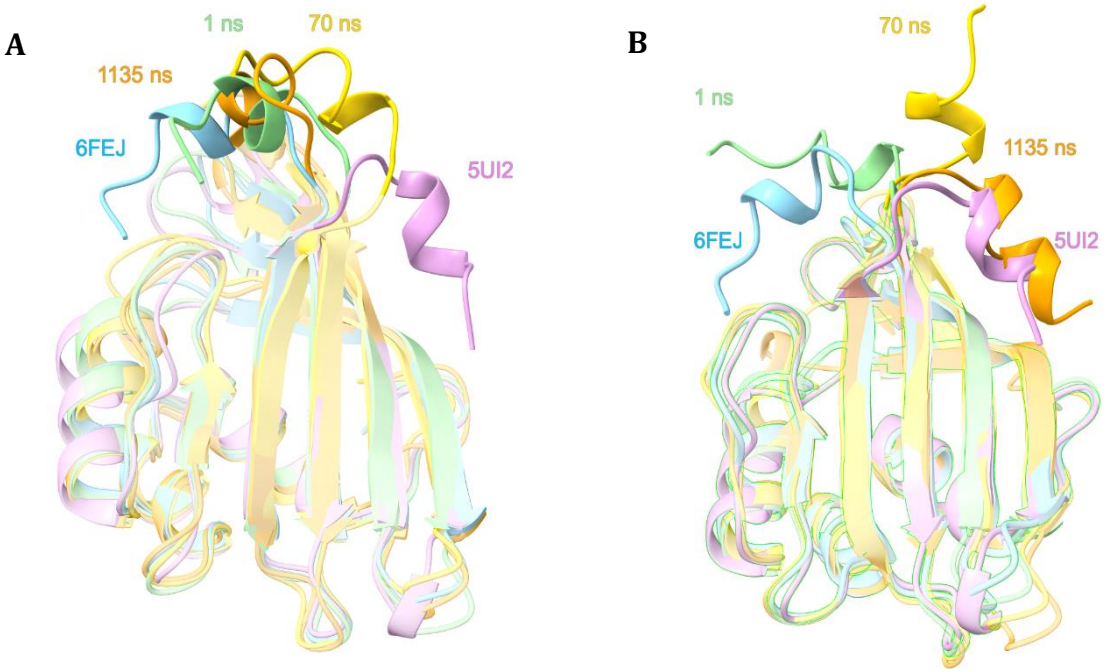

Figure 3. Molecular dynamics simulation of CTT conformational changes in apoCTDH. MD was performed multiple times resulting in two possible results see in panel A, where the CTT remains in its original closed position and panel B**,** where the CTT flips out to adopt the open position. In both A and B, frames presented were sampled at t = 1ns (green), t = 70 ns (gold) and t=1135 ns (orange). OCP^{O} CTD from PDB 5UI2 (violet) and CTDH structure PDB 6FEJ (cyan), are also shown for comparison. All panels show the protein in cartoon representation.

the pocket region without requiring major changes in the CTDH structure or by applying directional constraints (Fig. S1A), as evidenced by accommodation of the ligand in the pocket in its original PDB conformation. We then chose the lowest energy conformation pose (see Methods section) as the starting point for the protein-CAN complex MD simulation.

When docked into the carotenoid-binding cavity, the initial lowest-energy cluster had the carbonyl group of CAN pointing away from the conserved Trp110, that has been shown to be important for carotenoid binding [10,39]. However, upon initiation of the MD simulation, CAN quickly flips (56 ns into the simulation) to form a hydrogen bond with Trp110, which also moves towards the CAN molecule. This interaction is quite stable and persists throughout the entire 2 μs simulation (Fig. S1B). The CTT was tracked throughout MD simulations of both apoCTDH and holoCTDH, in order to explore whether CAN incorporation into the carotenoid-binding cavity induces different protein dynamics. Each variant was monitored for

six simulations (2 μs per run). In both cases, two classes of predominant conformations could be identified. In the first class, the CTT slightly moves towards the cavity entrance (Fig. 3A shows snapshots from a typical simulation for apoCTDH while Fig. S2A shows snapshots from a typical simulation for holoCTDH), but essentially remains in the same initial position (further referred to as the closed conformation). In the second class, the CTT flips out to the position seen for the CTT of CTD in the holoOCP^{O} state (referred to as the open position; Fig. 3B and Fig. S2B). To follow these trajectories quantitatively, we monitored the RMSD displacement of the CTT with respect to either the closed conformation in PDB 6FEJ (Fig. S3A, S3B for apoCTDH and S3E, S3F for holoCTDH) or the open conformation in 5UI2 (Fig. S3B S3C, S3D for apoCTDH and Fig. S3G, S3H for holoCTDH). In general, these complementary reference simulations show whether the CTT is flipped from the closed to the open position (Fig. S3A, S3C for apoCTDH and S3E, S3G for holoCTDH), or not (Fig. S3B, S3D for apoCTDH and S3F, S3H for holoCTDH). In both holoCTDH and apoCTDH, CTT flips in two independent runs (2 out of 6 runs ,33%), although in apoCTDH, one of the two flips is shorter and less stable and flips twice, from closed to open, then back to closed (Fig. S3A, S3C; pink trace). Careful examination of these RMSD traces implies the existence of a strong binding mode of the CTT by the outward-facing β-sheet, that in all cases resulted in a spatially similar state (RMSD = 5Å to the open position). Finally, an additional conformation emerged from the simulations - an intermediate perpendicular CTT position (gold in Fig. 3B), which has non-negligible occurrence, as the CTT dwells in this position before collapsing to one of the terminal positions (either open or closed). This perpendicular orientation is retained for much longer period in apoCTDH (Fig. S3A, S3C) as opposed to holoCTDH (Fig. S3E, S3G), as derived from the mid RMSD range (5Å<RMSD<15Å). This state is similar to the second population of the 6S5L structure (yellow in Fig. 2A), thus hinting at the possible relevancy of this state. We postulate that this CTT orientation might be relevant for extraction or delivery of the carotenoid, as it can

extend out towards a donating/receiving partner. The hinge point that allows this rotation of the CTT helix between the closed and open conformation is between A129 and S130. The phi and psi angles between those two residues change dramatically from -150 to 50 degrees and from -50 to -150 degrees respectively, to allow for the hinge movement (Fig. S4). Remarkably, in the apoCTDH simulations that result on the open state (Fig. S3A, S3C – red trace), the first 500ns are characterized by highly fluctuating RMSD values, despite almost no change in the dihedrals at the respective time frame (Fig. S4). At about 500ns, the dihedral angles change allowing CTT flip to its final, fully open position. The dramatic change in dihedral angles at the A129-S130 bond allows the CTT to adopt the fully open CTT conformation. Furthermore, the movement of the CTT into the open conformation of CTT is only possible in a monomer or by disrupting the back-to-back dimer interface, thus we performed additional simulations to study the putative mechanisms for back-to-back to head-to-head CTDH reorganization. Molecular Mechanics Poisson-Boltzmann Surface Area (MM-PBSA) calculation is a post-processing end-state method that can estimate the free energies of protein-ligand biding complexation process [40]. MM-PBSA results show that back-to-back interface is predicted to be very stable, as most AAs contribute substantial negative ΔG values, resulting in a $\Delta G_{dimerization}$ = -41 Kcal. (-20.5 Kcal/monomer). Furthermore, MM-PBSA allows to decompose calculated free energies and identify specific amino acids (AAs) that stabilize protein-protein interaction. This analysis (Fig. S5) reveals several residues that contribute more than -2 Kcal to the change in free energy upon complex formation of the back-to-back dimer (i.e. hot spots). These include L82, Q94, S96 and L109, which are found in the β-sheet forming the back-to-back interface (6FEJ monomer is shown in Fig. 4A).

After the CTT dwells and passes the interim perpendicular state (Fig. 4B), completing a full flip, it adopts the open conformation, in which L137 interacts with the same four hydrophobic AAs that stabilize the back-to-back dimerization

state (Fig. 4C) which remains fairly stable throughout the remainder of the simulation. In this open conformation, the CTT is virtually identical (structurally) to the same region in the crystal structure of holoCTD of OCP^{O} (5UI2, RMSD = 5Å), mentioned earlier in the text. Interestingly, the polar residues S96 and Q94, which initially pointed towards each other (O-O distance ~4.5 Å), now point away from each other (O-O distance now ~9 Å), making room for L137 and allowing the formation of this hydrophobic interaction. Notably, if a CTDH monomer with its opened CTT conformation is superimposed onto one of the back-to-back dimer monomers (Fig. 4D), the α-helix (positions 129 to 138) overlaps with the second monomer. Moreover, in the CTT open conformation, residue L137 overlaps with the interfacial residue L82 of the second monomer (Fig. 4D) "replacing" its stabilizing role between monomers, creating a transient internal hydrophobic patch that replaces the second monomer interface patch in a similar way. Therefore, we believe the CTT flip may have two inter-connected roles, a pigment ligand binding role and a complex formation role which combine to affects carotenoid uptake and delivery (see below).

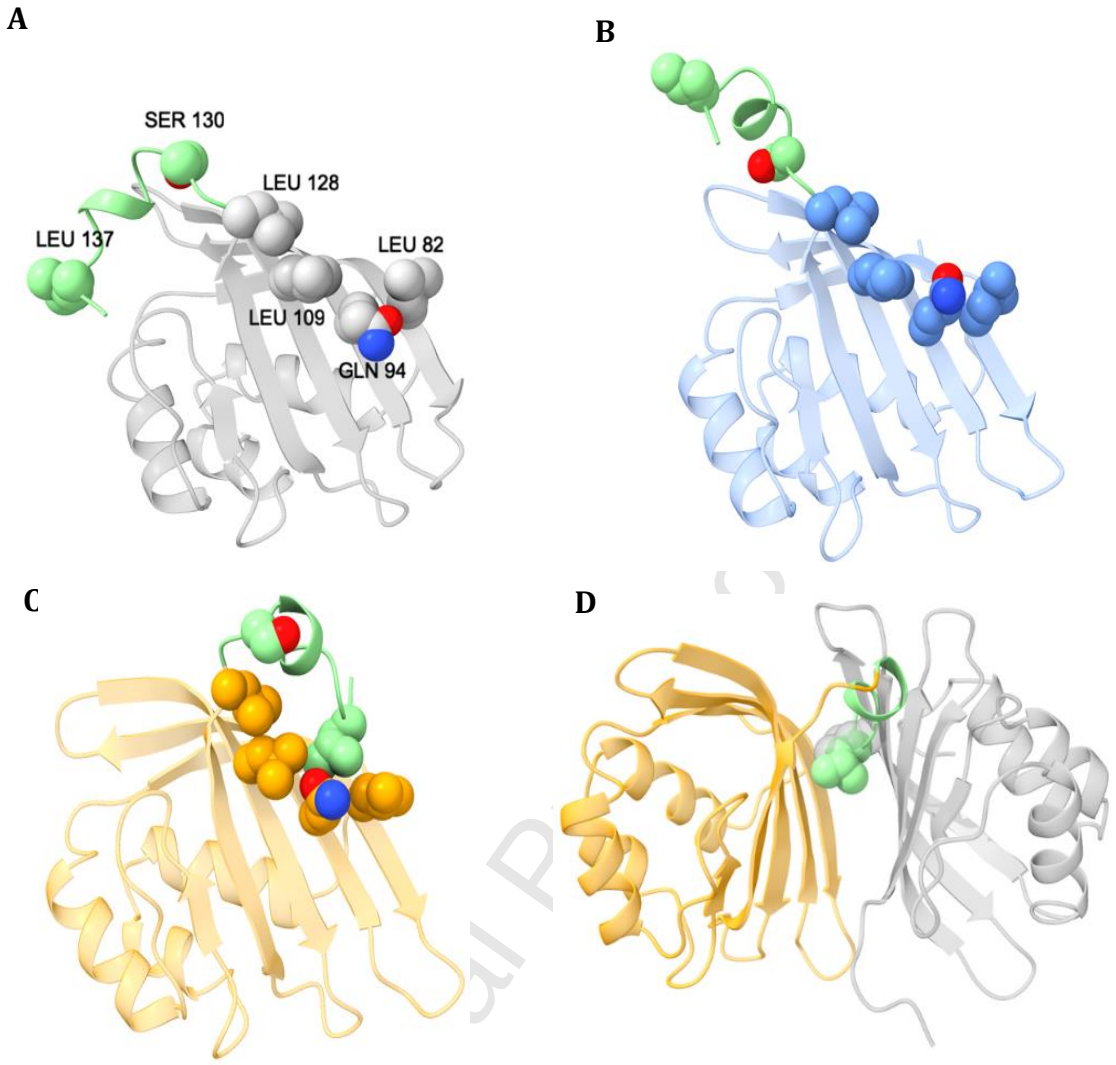

Figure 4. Molecular dynamics reveals how Leu137 stabilizes the "open" CTT position by forming an intramolecular hydrophobic cluster. (**A**) Initial MD apoCTDH monomer (carved from PDB 6FEJ), shows that while the CTT adopts the "closed" conformation, the stabilizing AAs (Leu128, Leu82, Leu109 and Asn94, spheres representation) are available to interact with the second monomer forming the back-to-back dimer (hidden for clarity). L137 is situated in the proximity of the carotenoid-binding cavity, well-away from the back-to-back interface (**B**) CTT intermediate conformation, perpendicularly to the CTDH globular protein. In this state, the CTT adopts the maximal reach for membrane incorporation, with L137 being the distal-most residue to the CTDH protein. (**C**) The CTT completes its movement and is stabilized in the "open" conformation. Ala129-Ser130 phi and psi are the dihedrals that are changed dramatically to allow hinge movement. In this orientation, Leu137 forms a hydrophobic cluster with the AAs formerly stabilizing the back-to-back interface, causing the CTT to be retained in the fully "open", bent, back-to-back destabilizing state. See Movie S1 for complete dynamic description of the CTT movement. (**D**) Upon translocation to the open conformation (orange cartoon), the CTT (green cartoon) is predicted to overlap with the second monomer (gray cartoon) forming the back-to-back interface, thus pushing it away. Then, the position of L137 (green spheres) of the first monomer overlaps with L82' (gray spheres) of the second monomer.

3.3 Combining mutagenesis and MD to probe ApoCTDH function

Analysis of the crystal structure, MMPBSA and MD simulations, enabled us to identify critical amino acids that participate in the back-to-back to head-to-head transition, as well as in carotenoid uptake and delivery. As indicated above, residues L128 and L137 appeared to be key in forming the open state and so we rationally introduced point mutations at these positions. L137 stands out structurally as the anchoring hook for the CTT movement to the open position by forming a hydrophobic cluster. Therefore, we replaced the Leucine with Aspartic acid at this site, to hamper the hydrophobic nesting feature. In addition, as demonstrated in our previous work, the CTT has a vital role in carotenoid uptake and delivery. Therefore, as L137 is the last hydrophobic residue of the CTT (before the hydrophilic RREQ-C-terminus), we expected that changing its nature would affect the CTDH function as well. We also hypothesized that L128 might have a prominent stabilizing effect on the back-to-back interface, based on the MMPBSA analysis and its position at the end of the β-strand from which the CTT protrudes. These mutations were added to our control CTDH, the C103F mutant. The replacement of C103 avoids the formation of C-C bonds between the CTDH monomers (see refs [36,37]) under oxidizing conditions. Thus, this mutation allows dimer opening and carotenoid dynamics under all redox conditions. SEC analysis (Fig. 5A) shows that the oligomeric state of holoCTDH is predominantly a dimer with the same overall size in the L137D and L128D mutants as well as the control protein. As can be expected, the ΔCTT mutant is noticeably smaller. However, the holo L128D CTDH mutant has an additional small population that was estimated to be the monomeric (Fig. S6), carotenoid-binding CTDH (similar to the *Thermosynechococcus elongatus* [36] CTDH). We attribute this behavior to a decrease in the CTT open position, as the CTT in the L128D mutant is less flexible. This hypothesis was then confirmed by MD simulations (Fig. S7A; Movie S2), showing that the CTT is "stuck" in a very stable intermediate, perpendicular

position, unable to complete the flip out to the open position. In contrast to the holoCTDH, when apoCTDH was analyzed (Fig. 5B), the

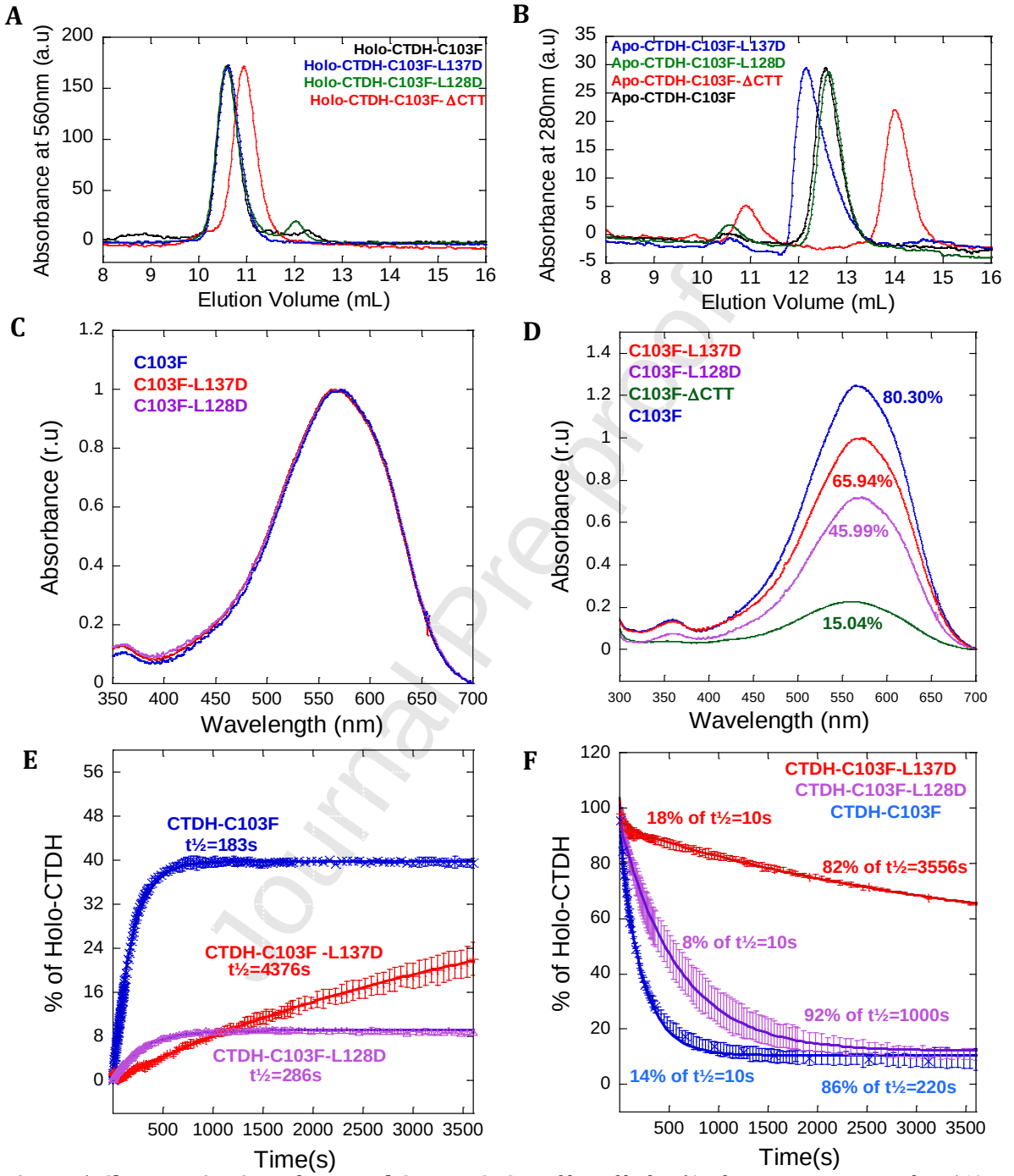

Figure 5. Characterization of mutated CTDHs. SEC profiles of holo- (A, absorption measured at 560 nm) and apo- (B, absorption measured at 280 nm) CTDHs (legend on graph). Markers and calibration curve can be found in Fig. S6 (C) Absorption spectra of mutated CTDHs. (D) Carotenoid uptake from carotenoid-containing membranes. Absorption spectra of the supernatant after 1 h incubation of canthaxanthin containing *E. coli* membranes with apoCTDH-C103F (blue curve), apoCTDH-C103F-L137D (red curve), apoCTDH-C103F-L128D (violet curve) and apoCTDH-C103F (green curve) after membrane removal. The % shown in the figure is the percentage of holoprotein at the end of incubation (E) Kinetics of carotenoid transfer from holoHCP1 to different mutated apoCTDHs. The ratio HCP1 to CTDH was 1:1 during the dark incubation. The time needed to transfer half of the maximum carotenoid transferred is marked in the figure. (F) Kinetics of carotenoid transfer from the different mutated holoCTDHs to apoHCP4, the ratio CTDH to HCP4 was 1:205 during the dark incubation. The kinetics presented show fast and slow phases. The $t_{1/2}$ for each phase is marked. The C103F mutation allows the separation of CTDH dimer and carotenoid transfer and uptake even under oxidizing conditions. The curves e and f are an average of three independent experiments. Error bars represent the standard deviation of the data.

oligomeric state was quite heterogeneous. Importantly, apoCTDH monomer/dimer ratio was shown to be concentration-dependent[35]. Therefore, we examined the relative impact of all mutations at the same intermediate concentration (10μM) that allows monomer/dimer equilibrium, to dissect the effect of the different mutations on the oligomeric state, and not the concentration effect. While the control protein (C103F) was shown to be predominantly a monomer, the ΔCTT mutant resulted in a substantial dimeric peak. We attribute this to the absence of the steric hindrance that the CTT imposes on the back-to-back interface upon flipping. Both L128D and L137D are predominantly monomers, with only very small dimeric fractions (much less than for the ΔCTT). Interestingly, the apo-L137D protein eluted faster through the column (with respect to control and L128D). This behavior was attributed to an increase in the hydrodynamic radius due to the enhanced dynamicity of CTT in this mutant, which stems from the loss of the CTT hydrophobic cluster anchor. This is expected to increase its mobility, allowing CTT to occupy a wider range of conformations, thus increasing its apparent volume. This hypothesis was also supported by three MD simulations of apoL137D (Fig. S7B), which reveals that the CTT flips more often than WT, including a double-flip (close-to-open-to-close) in one of them. This increased tendency of CTT flips (100% in apoCTDH-L137D vs. 33% in to apoCTDH control), hinting at the increased propensity of this mutant to go back-and-forth over the course of several minutes (elution in the column), resulting in increased apparent volume (Fig. S6). The loss of L137 seems to loosen the interaction of the CTT with the β5/β6 loop, thus enabling this flip with relative ease. Overall, this finding strongly corroborates our MD simulation-derived hypothesis, which suggests that the CTT is retained in the open position by L137 anchoring to the counter hydrophobic cluster tightly and specifically.

As the CTDH protein functions as a relay between carotenoid uptake and delivery, we were interested to examine how these point-mutations affect the ability of the apoCTDH mutants to extract a carotenoid from membranes or from HCP1 and the ability of the holoCTDH mutants to deliver a carotenoid to apoHCP4. We first examined whether introducing the L137D or L128D mutations affect protein-carotenoid interactions. The absorption spectra of holoCTDH for both mutations are essentially identical (Fig. 5C), suggesting that the protein-chromophore interaction remain similar in all forms of holoCTDH. However, these point mutations have a strong impact on all aspects of CTDH carotenoid-shuttling capabilities. The ability to uptake a carotenoid from membranes (Fig. 5D) is reduced by 14% in the case of L137D, and by 34% in L128D, as demonstrated in Fig. 5D. Complete truncation of the CTT results in an apoCTDH with poor ability to uptake a carotenoid from membranes (reduced by 65% compared to the WT case) (Fig 5D and [33]) . The reduction in uptake by L137D could be explained by the decrease in CTT hydrophobicity at the site most likely to interact with the carotenoid in the membrane. L128D also shows decreased functionality which cannot be explained in a similar fashion. Examination of the time-resolved results presented in Fig. 5E (carotenoid acquisition by apoCTDH from holoHCP1) and Fig. 5F (carotenoid delivery from holoCTDH to apoHCP4) enables a better understanding of the different effects these point mutations have. The L128D mutation impaired mainly the carotenoid uptaking that exhibits a decrease in amplitude, with kinetics similar to the control. In contrast, L137D as a very slow kinetics for both functions (Figs. 6E and F). Taken together we suggest that L128D mainly compromises CTT flexibility (possibly favoring the closed conformation), which is more crucial for carotenoid uptake (from membranes or holoHCP1) than delivering a carotenoid to a receiving entity (apoHCP4). As for L137D, introducing this hydrophobic/hydrophilic switch makes it challenging and kinetically slower for the hydrophobic carotenoid to slide past this point (either

on the way into CTDH carotenoid-binding cavity or from it), yet thermodynamically favorable (with respect to L128D).

4. Discussion

In this work, we have provided evidence for the dynamics in the CTDH structure that can control the change between the two functional dimeric organizations: either back-to-back (apoCTDH), or head-to-head orientation (as in holoCTDH or OCP^{O}). This was made possible by following the observations that emerged from the determination of the expanded oligomeric state apoCTDH structure. It is important to note that this expanded oligomeric state was already present in solution and is not a consequence of crystallization forces, as shown by SEC analysis in our previous work [33]. Moreover, it most likely would not have crystallized if this assembly was not the dominant population in solution. An interesting question that arises from the crystal structure presented here is whether the expanded assembly might have an important functional role *in-vivo*. OCP is constantly present (in its inactive OCP^{O} state) on the cytosolic side of the thylakoid membrane (in proximity to the PBS), anticipating an increase in light to be immediately activated into its OCP^{R} photo-protective state. We suggest that the expanded apoCTDH assembly may have similarities to the OCP^{O}. Increased illumination leading to high levels of photosynthesis might induce a transition into the active back-to-back dimers (as mimicked by the addition of 2M urea) perhaps as a result in a change in the pH of the cytosol, thus activating the carotenoid uptake mode by CTDH, in a fast-response manner, enabling consequent HCP activation for photo-protection.

The 12 CTTs in the expanded oligomeric apoCTDH are found in two different, intermediate positions with respect to holoCTD of OCP^O (open state) and the 2M urea apoCTDH (closed state). This almost movie-like superposition image of CTT movement emphasized that the CTT is highly flexible, leading us to the performance of the MD simulations technique to study this flexibility and its role in this protein's function. These simulations show that once the CTT reaches the open state, it is retained there for the entire duration of the simulation, stabilized by its anchoring to a tight hydrophobic cluster located on the putative dimer interface. We hypothesize that the presence of CAN may reduce the activation energy entailed in going from a "closed" CTT position (as in 6FEJ) to the "open" anchored position (as in OCP^O), thus facilitating the hinge movement. In addition, an intermediate, perpendicular state of the CTT was detected, which we propose to be the "active" mode of carotenoid uptake and delivery. We attribute the difference in dwelling time of the perpendicular CTT orientation between apo and holo forms, to the difference in the interacting partner. As carotenoid uptake is mainly done from membranes, the CTT also serves as the membrane-integrating feature of apoCTDH. Thus, the need to maintain this extended, perpendicular state for a long period of time is pivotal for successful association with the membrane. In contrast, carotenoid delivery is made to a protein entity (apoHCP4), thus the need to maintain the extended conformation by the CTT may be less critical, as other protein-protein stabilizing interactions might facilitate this interaction. The open state stabilization was shown to occur due to the anchoring of the L137 residue with the same hydrophobic cluster, which stabilizes the back-to-back dimeric interaction. Thus, a transition mechanism from a back-to-back mode to a head-to-head mode was hypothesized, suggesting that the CTT open state conformation imposes steric strain on the second monomer, pushing it away (Fig. 6). Point mutagenesis supports this hypothesis, showing that L137 serves as the anchoring hook of the CTT in the open state, as well as having a pivotal role in carotenoid delivery and uptake. On the other hand, L128 which has a stabilizing

effect on the back-to-back interaction and possibly on the closed CTT conformation, was shown to be specifically critical for carotenoid uptake, but less so for carotenoid delivery.

The structural mechanism for carotenoid uptake, binding and delivery revealed in this work may be extended to other systems, revealing a more general mechanism. The retinal pigment epithelium 65 (RPE65) enzyme is known to function as retinoid isomerase in the vertebrate visual system, binding an all-trans retinol as its substrate [41,42]. RPE65 must first uptake free retinol from membranes, in fashion similar to carotenoid uptake by the CTDH. The CTDH has been shown to be structurally homologous to nuclear transport factor 2 (NTF2) protein which is known to be a key relay for the trafficking of RanGDP into the nucleus, passing it on through the nuclear pore complex [43,44]. Both RPE65 and NTF2 are also predominantly dimeric and were shown to adopt back-to-back orientations *in crystal* [41,44]. However, in contrast to the dimeric CTDH, which has the cavities of its two dimer-forming monomers facing the opposite directions (anti-parallel back-to-back), the cavities of both RPE65 and NTF2 dimers face the same direction (parallel back-to-back). These differences may provide the rational for the different functions of these proteins, from the perspective of ligand dynamics. While the RPE65 dimer is an enzyme that catalyzes two stereospecific retinoid isomerizations and NTF2 dimer binds two RanGDP proteins (via the Phe72-containing loop of RanGDP), CTDH is an interim relay for a single CAN cargo. Therefore, while for RPE65 and NTF2 the main feature is maximizing cargo loading, for CTDH it is rather the delicate control over the uptake and delivery of carotenoid cargo. Had the CTDH dimer cavities faced the same direction (as in RPE65 and NTF2), the multiple CAN uptake would have prevented the encapsulation of one carotenoid by two monomers in the head-to-head orientation, as two carotenoids could have been extracted simultaneously. This would result in decreased stability of the protein-ligand interaction, as the length of the CAN ligand is twice the size of the cavity found in one monomer.

Therefore, we propose that the anti-parallel orientation of apoCTDH dimer is evolutionarily designed to allow only one monomer to extract a single carotenoid from the membrane at a given time. Then, through the mechanism discussed in this work, the second monomer (which is still carotenoid-free thanks to the anti-parallel orientation) is isomerized to encapsulate the carotenoid following the CTT-induced back-to-back dimer destabilization (Fig. 6).

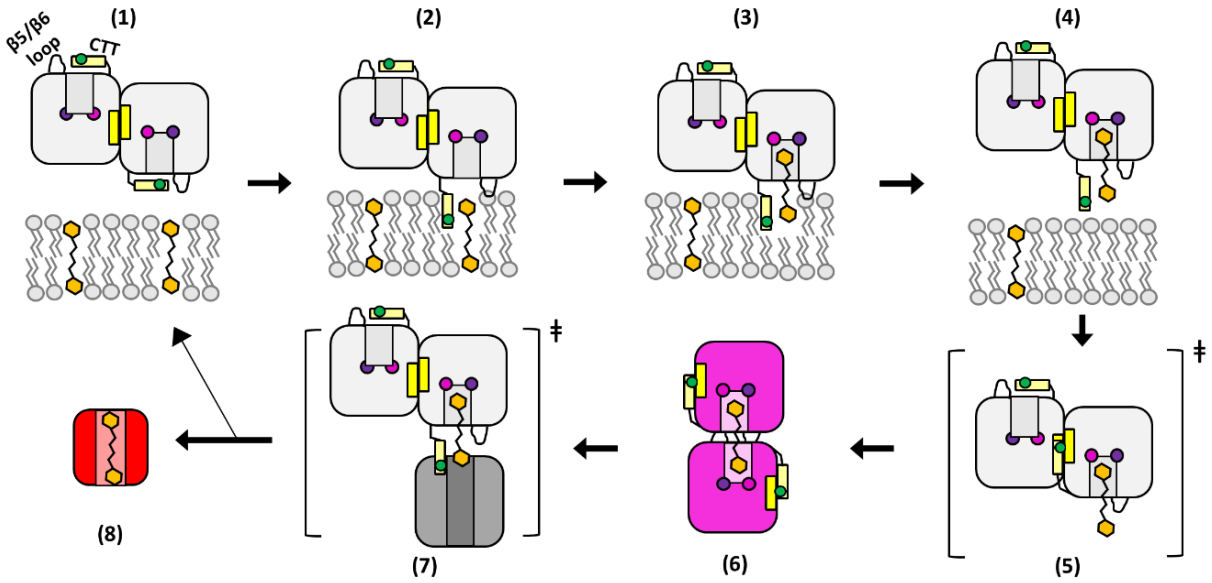

Figure 6. Structural dynamics enabling carotenoid relay (depicted in Sluchanko-Maksimov representation). (**A**) Carotenoid relay cycle by the CTDH starts with a back-to-back dimer (1) incorporating its CTT into the membrane to extract a carotenoid, with the assistance of L137, depicted in brown circle (2). Then, the carotenoid is bound via the conserved hydrogen bonding formed by residues Trp110 and Phe27, depicted in blue and purple circles (3). The dimer then leaves the membrane vicinity (4) and the uptake process may facilitate the complete CTT hinge movement, pushing it outside to form a metastable state where steric hindrance occurs between the CTT and the second monomer. In addition, the CTT now satisfies in an intramolecular fashion (using L137) the previously back-to-back forming β-sheet, depicted in yellow rectangles (5). This results in quaternary structure isomerization (face-to-face dimer), yielding the holoCTDH, which has a violet color in solution (6). Upon interaction with apoHCP or apoOCP (7), the carotenoid is delivered, forming a red-colored protein in solution (8), leaving the apoCTDH back-to-back dimer to regenerate the cycle (1).

In addition, we propose that the CTT-induced destabilization for CTDH is the same one governing the monomerization of the NTF2 dimer, which was shown to be important for RanGDP release [44]. Having such a conserved fold retained across the two super-kingdoms of life (prokaryotes and eukaryotes), which is evolutionary designated for delivering a cargo from one place to another, is most likely not just a coincidence. Being structurally highly homologous (Fig. S8), it is reasonable to assume that these proteins share not only rigid structural motif, but rather structural dynamics motif, as they both perform similar functions. Point mutations replacing hydrophobic side chains with charged ones in the interface between the parallel back-to-back NTF2 dimer was shown to decrease the back-to-back NTF2 dimer stability [43]. We suggest that these mutations are equivalent of the CTT flip in the wild-type NTF2, i.e. weakening the back-to-back interaction, thus echoes the behavior demonstrated in this endeavor for CTDH.

In conclusion, a novel quaternary-structure reorganization process of carotenoid-binding protein was discovered, emphasizing the importance of dynamics on protein-ligand regulation, as well as unraveling critical roles of specific amino acids in this carotenoid uptake and delivery mechanism.

5. Acknowledgements

The coordinates of the expanded oligomeric state apoCTDH structure has been deposited in the Protein Data Bank under accession code 6S5L. This work was supported by the Israel Science Foundation founded by the Israel Academy of Sciences and Humanities (843/16), grants from the Agence Nationale de la Recherche RECYFUEL [ANR-16-CE05-0026]) and by the European Union's Horizon 2020 research and innovation program under grant agreement no.675006 (SE2B). F.M.'s salary is financed by SE2B. The research is also supported by the Centre National de la Recherche Scientifique and the Commissariat à l'Energie Atomique. The French Infrastructure for Integrated Structural Biology (FRISBI) ANR-10-INBS-05 also partially supported this research. We gratefully thank Dr. Yael Pazy-Benhar and Dikla Haya of Technion Center for Structural Biology (TCSB) for assisting with radiation facilities and data collection.

6. References

[1] R. Croce, R. Van Grondelle, H. Van Amerongen, I. Van Stokkum, Light Harvesting in Photosynthesis, 1st ed., CRC Press, 2018.

[2] H.A. Frank, A. Cua, V. Chynwat, A. Young, D. Gosztola, M.R. Wasielewski, Photophysics of the carotenoids associated with the xanthophyll cycle in photosynthesis, Photosynth. Res., 41 (1994) 389–395.

[3] B.R. Green, D.G. Durnford, The chlorophyll-carotenoid proteins of oxygenic photosynthesis, Annu. Rev. Plant Biol., 47 (1996) 685–714.

[4] B.W. Dreyfuss, J.P. Thornber, Assembly of the light-harvesting complexes (LHCs) of photosystem II (monomeric LHC Iib complexes are intermediates in the formation of oligomeric LHC IIb complexes), Plant Physiol., 106 (1994) 829–839.

[5] A. Röding, E. Boekema, C. Büchel, The structure of FCPb, a light-harvesting complex in the diatom Cyclotella meneghiniana, Photosynth. Res., 135 (2018)

203–211.

[6] R.E. Blankenship, Origin and early evolution of photosynthesis, Photosynth. Res., 33 (1992) 91–111.

[7] R.E. Blankenship, H. Hartman, The origin and evolution of oxygenic photosynthesis, Trends Biochem Sci, 23 (1998) 94–97.

[8] C.A. Kerfeld, Water-soluble carotenoid proteins of cyanobacteria, Arch. Biochem. Biophys., 430 (2004) 2–9.

[9] A. Wilson, G. Ajlani, J.M. Verbavatz, I. Vass, C.A. Kerfeld, D. Kirilovsky, A soluble carotenoid protein involved in phycobilisome-related energy dissipation in cyanobacteria, Plant Cell, 18 (2006) 992–1007.

[10] D. Kirilovsky, C.A. Kerfeld, The Orange Carotenoid Protein: a blue-green light photoactive protein, Photochem Photobiol Sci, 12 (2013) 1135–1143.

[11] D. Kirilovsky, C.A. Kerfeld, Cyanobacterial photoprotection by the orange carotenoid protein, Nat Plants, 2 (2016) 16180.

[12] D. Kirilovsky, Photoprotection in cyanobacteria: The orange carotenoid protein (OCP)-related non-photochemical-quenching mechanism, Photosynth. Res., 93 (2007) 7–16.

[13] D. Kirilovsky, Modulating energy arriving at photochemical reaction centers: orange carotenoid protein-related photoprotection and state transitions, Photosynth Res, 126 (2015) 3–17.

[14] A. Wilson, C. Punginelli, A. Gall, C. Bonetti, M. Alexandre, J.M. Routaboul, C.A. Kerfeld, R. van Grondelle, B. Robert, J.T. Kennis, D. Kirilovsky, A photoactive carotenoid protein acting as light intensity sensor, Proc Natl Acad Sci U S A, 105 (2008) 12075–12080.

[15] A. Wilson, J.N. Kinney, P.H. Zwart, C. Punginelli, S. D'Haene, F. Perreau, M.G. Klein, D. Kirilovsky, C.A. Kerfeld, Structural determinants underlying photoprotection in the photoactive orange carotenoid protein of cyanobacteria, J Biol Chem, 285 (2010) 18364–18375.

[16] H. Zhang, H. Liu, D.M. Niedzwiedzki, M. Prado, J. Jiang, M.L. Gross, R.E. Blankenship, Molecular mechanism of photoactivation and structural location of the cyanobacterial orange carotenoid protein, Biochemistry, 53 (2014) 13–19.

[17] C.A. Kerfeld, M.R. Melnicki, M. Sutter, M.A. Dominguez-Martin, Structure, function and evolution of the cyanobacterial orange carotenoid protein and its homologs, New Phytol., 215 (2017) 937–951.

[18] R.L.L. Leverenz, M. Sutter, A. Wilson, S. Gupta, A. Thurotte, C.B. de Carbon, C.J.J. Petzold, C. Ralston, F. Perreau, D. Kirilovsky, C. Bourcier de Carbon, C.J.J. Petzold, C. Ralston, F. Perreau, D. Kirilovsky, C.A. Kerfeld, A 12 A carotenoid translocation in a photoswitch associated with cyanobacterial photoprotection, Science (80-.)., 348 (2015) 1463–1466.

[19] P.E. Konold, I.H.M. Van Stokkum, F. Muzzopappa, A. Wilson, M.-L. Groot, D. Kirilovsky, J.T.M. Kennis, Photoactivation mechanism, timing of protein secondary structure dynamics and carotenoid translocation in the Orange Carotenoid Protein, J. Am. Chem. Soc., 141 (2018) 520–530.

[20] S. Bandara, Z. Ren, L. Lu, X. Zeng, H. Shin, K.-H. Zhao, X. Yang, Photoactivation mechanism of a carotenoid-based photoreceptor, Proc. Natl. Acad. Sci. U. S. A., 114 (2017) 6286–6291.

[21] R.L. Leverenz, D. Jallet, M.D. Li, R.A. Mathies, D. Kirilovsky, C.A. Kerfeld, Structural and functional modularity of the orange carotenoid protein: distinct roles for the N- and C-terminal domains in cyanobacterial photoprotection, Plant Cell, 26 (2014) 426–437.

[22] E.G. Maksimov, N.N. Sluchanko, K.S. Mironov, E.A. Shirshin, K.E. Klementiev, G. V Tsoraev, M. Moldenhauer, T. Friedrich, D.A. Los, S.I. Allakhverdiev, Fluorescent labeling preserving OCP photoactivity reveals its reorganization during the photocycle, Biophys. J., 112 (2017) 46–56.

[23] D. Harris, O. Tal, D. Jallet, A. Wilson, D. Kirilovsky, N. Adir, Orange carotenoid protein burrows into the phycobilisome to provide photoprotection, Proc. Natl. Acad. Sci. U. S. A., 113 (2016) E1655–E1662.

[24] M. Gwizdala, A. Wilson, D. Kirilovsky, In vitro reconstitution of the cyanobacterial photoprotective mechanism mediated by the Orange Carotenoid Protein in Synechocystis PCC 6803, Plant Cell, 23 (2011) 2631–2643.

[25] R. Berera, I.H.M. Van Stokkum, J.T.M. Kennis, R. Van Grondelle, J.P. Dekker, The light-harvesting function of carotenoids in the cyanobacterial stress-inducible IsiA complex, Chem. Phys., 373 (2010) 65–70.

[26] A.H. Squires, P.D. Dahlberg, H. Liu, N.C.M. Magdaong, R.E. Blankenship, W.E. Moerner, Single-molecule trapping and spectroscopy reveals photophysical heterogeneity of phycobilisomes quenched by Orange Carotenoid Protein, Nat. Commun., 10 (2019) 1172.

[27] C.A. Kerfeld, M.R. Sawaya, V. Brahmandam, D. Cascio, K.K. Ho, C.C. Trevithick-Sutton, D.W. Krogmann, T.O. Yeates, The crystal structure of a cyanobacterial water-soluble carotenoid binding protein, Structure, 11 (2003) 55–65.

[28] R. Lopez-Igual, A. Wilson, R.L. Leverenz, M.R. Melnicki, C. Bourcier de Carbon, M. Sutter, A. Turmo, F. Perreau, C.A. Kerfeld, D. Kirilovsky, Different Functions of the Paralogs to the N-Terminal Domain of the Orange Carotenoid Protein in the Cyanobacterium Anabaena sp PCC 7120, Plant Physiol, 171 (2016) 1852–1866.

[29] H. Bao, M.R. Melnicki, C.A. Kerfeld, Structure and functions of Orange Carotenoid Protein homologs in cyanobacteria, Curr. Opin. Plant Biol., 37 (2017) 1–9.

[30] M.R. Melnicki, R.L. Leverenz, M. Sutter, R. Lopez-Igual, A. Wilson, E.G. Pawlowski, F. Perreau, D. Kirilovsky, C.A. Kerfeld, Structure, Diversity, and Evolution of a New Family of Soluble Carotenoid-Binding Proteins in Cyanobacteria, Mol Plant, 9 (2016) 1379–1394.

[31] M. Sutter, A. Wilson, R.L. Leverenz, R. Lopez-Igual, A. Thurotte, A.E. Salmeen, D. Kirilovsky, C.A. Kerfeld, Crystal structure of the FRP and identification of the active site for modulation of OCP-mediated photoprotection in cyanobacteria, Proc Natl Acad Sci U S A, 110 (2013) 10022–10027.

[32] A. Sedoud, R. Lopez-Igual, A. Ur Rehman, A. Wilson, F. Perreau, C. Boulay, I. Vass, A. Krieger-Liszkay, D. Kirilovsky, The Cyanobacterial Photoactive Orange Carotenoid Protein Is an Excellent Singlet Oxygen Quencher, Plant Cell, 26 (2014) 1781–1791.

[33] D. Harris, A. Wilson, F. Muzzopappa, N.N. Sluchanko, T. Friedrich, E.G. Maksimov, D. Kirilovsky, N. Adir, Structural rearrangements in the C-terminal domain homolog of Orange Carotenoid Protein are crucial for carotenoid transfer, Commun. Biol., 1 (2018) 125.

[34] E.G. Maksimov, N.N. Sluchanko, Y.B. Slonimskiy, K.S. Mironov, K.E. Klementiev, M. Moldenhauer, T. Friedrich, D.A. Los, V.Z. Paschenko, A.B. Rubin, The Unique Protein-to-Protein Carotenoid Transfer Mechanism, Biophys. J., 113 (2017) 402–414.

[35] M. Moldenhauer, N.N. Sluchanko, D. Buhrke, D. V Zlenko, N.N. Tavraz, F.J. Schmitt, P. Hildebrandt, E.G. Maksimov, T. Friedrich, Assembly of photoactive orange carotenoid protein from its domains unravels a carotenoid shuttle mechanism, Photosynth. Res., 133 (2017) 327–341.

[36] F. Muzzopappa, A. Wilson, V. Yogarajah, S. Cot, F. Perreau, C. Montigny, C. Bourcier de Carbon, D. Kirilovsky, The paralogs to the C-terminal domain of the cyanobacterial OCP are carotenoid donors to HCPs, Plant Physiol., (2017) pp.01040.2017.

[37] Y.B. Slonimskiy, F. Muzzopappa, E.G. Maksimov, A. Wilson, T. Friedrich, D. Kirilovsky, N.N. Sluchanko, Light-controlled carotenoid transfer between water-soluble proteins related to cyanobacterial photoprotection, FEBS J., (2019).

[38] O. Trott, A.J. Olson, AutoDock Vina: improving the speed and accuracy of docking with a new scoring function, efficient optimization, and multithreading, J. Comput. Chem., 31 (2010) 455–461.

[39] N.N. Sluchanko, K.E. Klementiev, E.A. Shirshin, G. V Tsoraev, T. Friedrich, E.G. Maksimov, The purple Trp288Ala mutant of Synechocystis OCP persistently quenches phycobilisome fluorescence and tightly interacts with FRP, Biochim. Biophys. Acta (BBA)-Bioenergetics, 1858 (2017) 1–11.

[40] S. Genheden, U. Ryde, The MM/PBSA and MM/GBSA methods to estimate ligand-binding affinities, Expert Opin. Drug Discov., 10 (2015) 449–461.

[41] P.D. Kiser, M. Golczak, D.T. Lodowski, M.R. Chance, K. Palczewski, Crystal structure of native RPE65, the retinoid isomerase of the visual cycle, Proc. Natl. Acad. Sci., 106 (2009) 17325–17330.

[42] P.D. Kiser, E.R. Farquhar, W. Shi, X. Sui, M.R. Chance, K. Palczewski, Structure of RPE65 isomerase in a lipidic matrix reveals roles for phospholipids and iron in catalysis, Proc. Natl. Acad. Sci., 109 (2012) E2747–E2756.

[43] C. Chaillan-Huntington, P.J.G. Butler, J.A. Huntington, D. Akin, C. Feldherr, M. Stewart, NTF2 monomer-dimer equilibrium, J. Mol. Biol., 314 (2001) 465–477.

[44] M. Stewart, H.M. Kent, A.J. McCoy, Structural basis for molecular recognition between nuclear transport factor 2 (NTF2) and the GDP-bound form of the Ras-family GTPase Ran, J. Mol. Biol., 277 (1998) 635–646.

[45] A.G.W. Leslie, Recent changes to the MOSFLM package for processing film and image plate data , Jt. CCP4 + ESF-EAMCB Newsl. Protein Crystallogr., No. 26. (1992).

[46] A.J. McCoy, R.W. Grosse-Kunstleve, P.D. Adams, M.D. Winn, L.C. Storoni, R.J. Read, Phaser crystallographic software, J. Appl. Crystallogr., 40 (2007) 658–674.

[47] P. V Afonine, R.W. Grosse-Kunstleve, N. Echols, J.J. Headd, N.W. Moriarty, M. Mustyakimov, T.C. Terwilliger, A. Urzhumtsev, P.H. Zwart, P.D. Adams, Towards automated crystallographic structure refinement with phenix refine, Acta Crystallogr. Sect. D Biol. Crystallogr., 68 (2012) 352–367.

[48] P. Emsley, K. Cowtan, Coot: model-building tools for molecular graphics, Acta Crystallogr D Biol Crystallogr, 60 (2004) 2126–2132.

[49] R.P. Joosten, F. Long, G.N. Murshudov, A. Perrakis, The PDB_REDO server for macromolecular structure model optimization, IUCrJ, 1 (2014) 213–220.

[50] W.L. DeLano, The PyMOL Molecular Graphics System (2002) DeLano Scientific, Palo Alto, CA, USA http://www.pymol.org, (2002).

[51] S. Release, 1: Maestro, Schrödinger, LLC, New York, NY, USA, (2016).

[52] J. Gasteiger, M. Marsili, Iterative partial equalization of orbital electronegativity—a rapid access to atomic charges, Tetrahedron, 36 (1980) 3219–3228.

[53] J. Wang, W. Wang, P.A. Kollman, D.A. Case, Antechamber: an accessory software package for molecular mechanical calculations, J. Am. Chem. Soc, 222 (2001) U403.

[54] J. Wang, R.M. Wolf, J.W. Caldwell, P.A. Kollman, D.A. Case, Development and testing of a general amber force field, J. Comput. Chem., 25 (2004) 1157–1174.

[55] D.A. Case, T.E. Cheatham III, T. Darden, H. Gohlke, R. Luo, K.M. Merz Jr, A. Onufriev, C. Simmerling, B. Wang, R.J. Woods, The Amber biomolecular simulation programs, J. Comput. Chem., 26 (2005) 1668–1688.

[56] H. Nguyen, J. Maier, H. Huang, V. Perrone, C. Simmerling, Folding simulations for proteins with diverse topologies are accessible in days with a physics-based force field and implicit solvent, J. Am. Chem. Soc., 136 (2014) 13959–13962.

[57] D.R. Roe, T.E. Cheatham III, PTRAJ and CPPTRAJ: software for processing and analysis of molecular dynamics trajectory data, J. Chem. Theory Comput., 9 (2013) 3084–3095.

[58] W. Humphrey, A. Dalke, K. Schulten, VMD: visual molecular dynamics, J. Mol. Graph., 14 (1996) 33–38.

[59] P.A. Kollman, I. Massova, C. Reyes, B. Kuhn, S. Huo, L. Chong, M. Lee, T. Lee, Y. Duan, W. Wang, Calculating structures and free energies of complex molecules: combining molecular mechanics and continuum models, Acc. Chem. Res., 33 (2000) 889–897.

[60] T.D. Goddard, C.C. Huang, E.C. Meng, E.F. Pettersen, G.S. Couch, J.H. Morris, T.E. Ferrin, UCSF ChimeraX: Meeting modern challenges in visualization and analysis, Protein Sci., 27 (2018) 14–25.

Declaration of interests

☒ The authors declare that they have no known competing financial interests or personal relationships that could have appeared to influence the work reported in this paper.

☐The authors declare the following financial interests/personal relationships which may be considered as potential competing interests:

Graphical abstract

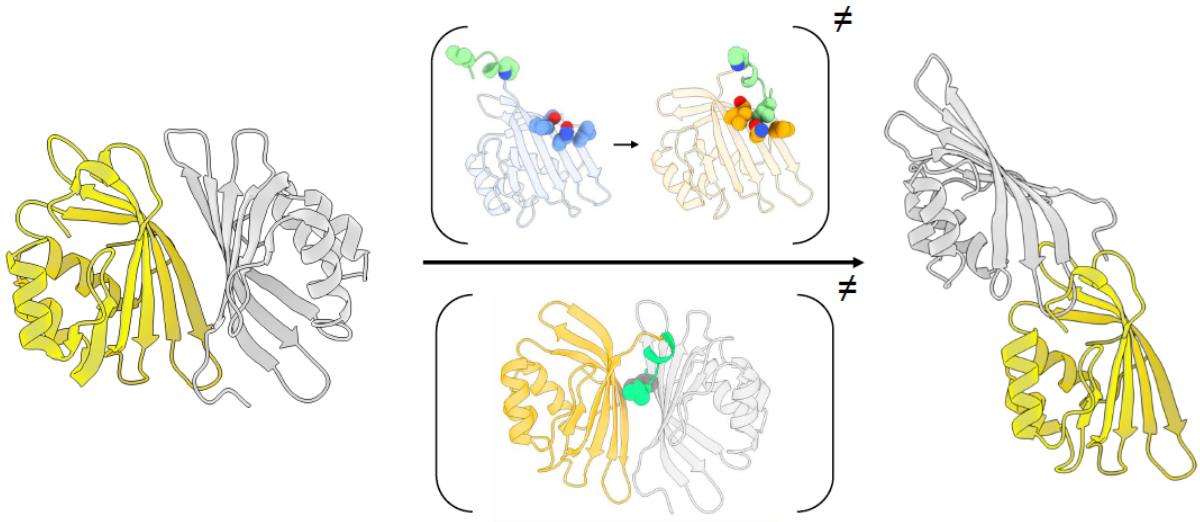

Highlights

- The C-terminal domain homolog (CTDH) of cyanobacterial OCP uptakes carotenoids from membranes.
- The crystal structure of the *Anabaena* CTDH protein reveals C-terminal tail dynamics.
- Molecular dynamics simulations reveal critical residues necessary for this dynamic behavior.
- Mutagenesis of these residues show impairment of carotenoid uptake and delivery by the CTDH.
- The mechanism of uptake and transfer of hydrophobic carotenoids by soluble proteins is proposed.